

Iterative Detection and Decoding for the Four-Rectangular-Grain TDMR Model

Michael Carosino

School of Electrical Engineering
and Computer Science
Washington State University
Pullman, WA, 99164-2752
Email: mcarosin@eecs.wsu.edu

Yiming Chen

Western Digital Corporation
Irvine, CA, 92612, USA
Email: yiming.chen@wdc.com

Benjamin J. Belzer,

Krishnamoorthy Sivakumar,
Jacob Murray and Paul Wettin
School of Electrical Engineering
and Computer Science
Washington State University
Pullman, WA, 99164-2752

Email: belzer,siva,jmurray,pwettin@eecs.wsu.edu

Abstract—This paper considers detection and error control coding for the two-dimensional magnetic recording (TDMR) channel modeled by the two-dimensional (2D) four-rectangular-grain model proposed by Kavcic, Huang et. al. in 2010. This simple model captures the effects of different 2D grain sizes and shapes, as well as the TDMR grain overwrite effect: grains large enough to be written by successive bits retain the polarity of only the last bit written. We construct a row-by-row BCJR detection algorithm that considers outputs from two rows at a time over two adjacent columns, thereby enabling consideration of more grain and data states than previously proposed algorithms that scan only one row at a time. The proposed algorithm employs soft-decision feedback of grain states from previous rows to aid the estimation of current data bits and grain states. Simulation results using the same average coded bit density and serially concatenated convolutional code (SCCC) as a previous paper by Pan, Ryan, et. al. show gains in user bits/grain of up to 6.7% over the previous work when no iteration is performed between the TDMR BCJR and the SCCC, and gains of up to 13.4% when the detector and the decoder iteratively exchange soft information.

Keywords—Two-dimensional magnetic recording, iterative detection and decoding, rectangular grain model

I. INTRODUCTION

Industry is approaching the limit of the data storage density possible on magnetic disk drives that write and read data on one-dimensional tracks. Intensive efforts are underway in alternative technologies such as heat-assisted-magnetic-recording (HAMR) and bit patterned media recording (BPM). Most of these techniques require the recording medium to be radically redesigned [1], and it is uncertain whether they will come on line quickly enough to prevent a plateau in magnetic disk storage density in the near to medium term.

This paper considers detection and coding techniques for an alternate approach proposed in [1] called two dimensional magnetic recording (TDMR), wherein bits are read and written in two dimensions on conventional magnetic hard disks. These disks have magnetic grains of different sizes packed randomly onto the disk surface. In TDMR, information bits are channel coded to a density of up to two bits per magnetic grain, and written by a special shingled write process that enables high density recording. A key problem is that a given magnetic grain retains the polarization of the last bit written on it; hence, if a grain is large enough to contain two bit centers, the oldest bit will be overwritten by the newer one.

A relatively simple model that captures the 2D nature of the TDMR channel is the four-grain rectangular discrete-grain model (DGM) introduced in [2], wherein four different grain types are constructed from one, two, or four small square tiles. In [2], capacity upper and lower bounds for this model are derived showing a potential density of 0.6 user bits per grain, translating to 12 Terabits/in² at typical media grain densities of 20 Teragrains/in². This is more than an order of magnitude improvement over current hard disk drives, which exceed densities of 500 Gigabits/in² [3].

Coding and detection for the four-grain DGM is considered in a previous paper by Pan, Ryan, et. al. [3]. They construct a BCJR [4] detection algorithm that scans the input image one row (track) at a time. A 16-state trellis is constructed as the Cartesian product of media states (that capture transitions between different grain geometries during a one tile move along a row) and data states (that capture the grain overwrite effect). It is shown that the number of states can be reduced to 6 by combining equivalent states. After one forward-backward pass through each row of the input image, the TDMR detector passes soft information in the form of log-likelihood ratios (LLRs) to a rate 1/4 serially concatenated convolutional code (SCCC) with puncturing, which decodes the data at the highest rate that achieves a bit error rate (BER) of 10⁻⁵ (corresponding to the highest possible user bit density.) No iteration between the TDMR detector and SCCC is done in [3], although the possibility is mentioned.

This paper proposes a two-row BCJR detector for the four-grain TDMR channel model. The novel contributions are as follows: 1.) Considering the outputs of two rows and two columns resulting from bits written on three input rows leads to a larger trellis with more grain configurations, enabling an increase in channel coding rates by up to 6.7% over [3]; 2.) Soft decision feedback of grain state information from

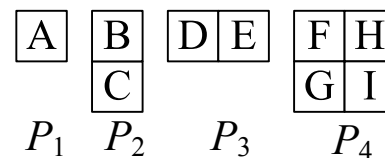


Fig. 1. Four-grain rectangular discrete grain model assumed in this paper, from [2].

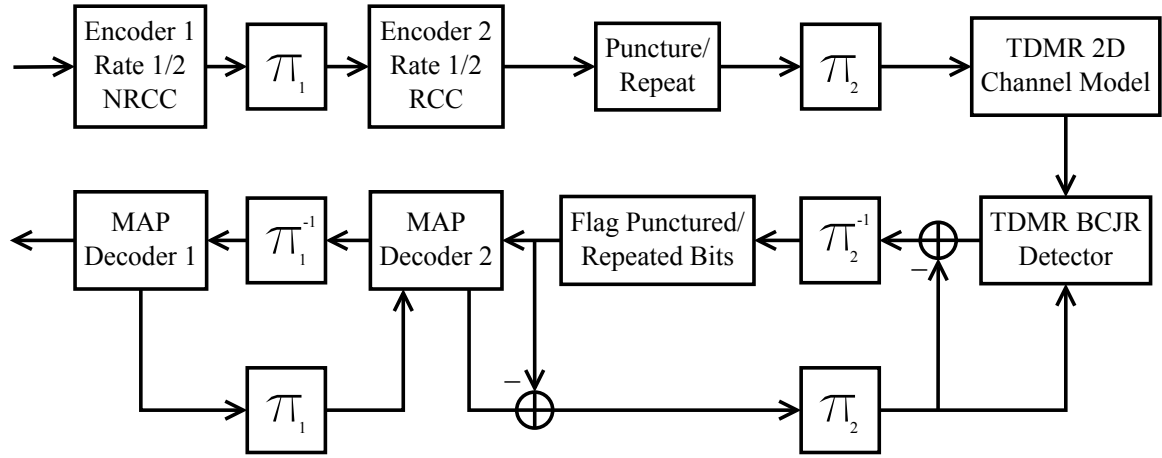


Fig. 2. Block diagram of transmitter and receiver for SCCC coded TDMR with iterative detection and decoding, after [3].

previously processed rows is used to aid the estimation of bits on the current rows; 3.) States are labeled and enumerated to avoid geometrically invalid states; 4.) By allowing the TDMR detector and SCCC decoder to iteratively exchange LLRs, code rate increases of up to 13.4% over [3] are achieved.

This paper is organized as follows. Section II summarizes the four grain DGM and gives an overview of the proposed system architecture. Section III explains the TDMR detection BCJR algorithm. Section IV describes simulation experiments, and section V concludes the paper.

II. CHANNEL MODEL AND SYSTEM ARCHITECTURE

As shown in Fig. 1, the rectangular DGM consists of four distinct grain types consisting of unions of the smallest grain type; relative to the smallest type their sizes are 1×1 , 2×1 , 1×2 and 2×2 . The four grain types occur with probabilities P_1, \dots, P_4 . In this paper it is assumed that there is one channel coded bit per 1×1 grain, and that the average number of coded bits per grain is 2, i.e., $1P_1 + 2P_2 + 2P_3 + 4P_4 = 2$. Hence, if the channel coding rate is r user bits per coded bit, the average number of user bits per grain is $2r$. The symmetry condition $P_2 = P_3$ is also assumed; this, together with the two bits per grain condition, allows the probabilities P_1 and P_4 to be computed given any valid value of $P_2 = P_3$. The rectangular grains are packed at random according to their probabilities into a 256×512 coded bit image, which models the magnetic disk surface, such that every location (m, n) in the image is covered by a grain or part of a grain. The subgrain labels A-F are used in the BCJR trellis definition described in subsection III-A.

The system architecture employed in this paper is shown in Fig. 2. A block of 32768 user information bits is encoded by a rate 1/4 SCCC from [5] consisting of an eight state rate 1/2 outer non-recursive convolutional code (NRCC) with generator matrix $G_1(X) = [1 + X, 1 + X + X^3]$, followed by an interleaver π_1 , followed by an inner eight state recursive systematic convolutional code (RCC) with generator matrix $G_2(X) = [1, (1 + X + X^3)/(1 + X)]$, followed by a second interleaver π_2 . Code rates greater than (respectively, less than) 1/4 are achieved by randomly puncturing (respectively, repeating) randomly selected output bits from the inner encoder. The

code, input block size, puncturing/repeat scheme and output block dimensions were chosen to be identical to those in [3] in order to facilitate comparison of the TDMR detector proposed in this paper with that in [3]. The TDMR channel model writes coded bits taking the values ± 1 onto the 256×512 coded bit image row-by-row in raster scan order, with multi-bit grains taking the sign of the last bit written on them. For example, all four bits of the grain labeled “FGHI” in Fig. 1 become equal to the bit written on its “I” subgrain, as this subgrain is farthest to the right and lowest and hence is the the last written.

The lower half of Fig. 2 depicts the iterative detection and decoding process. In the first outer iteration of the entire system, the coded bit image from the TDMR channel is read into the TDMR BCJR detector, which outputs channel bit LLRs to the inner MAP decoder. The inner MAP then exchanges LLRs with the outer MAP decoder for several iterations before passing back estimates of the code bit LLRs to the TDMR detector, and then another outer iteration of the entire detector/decoder is started. After several outer iterations, the outer decoder puts out the decoded user bits. Subtraction of incoming extrinsic information is performed at the outputs of the TDMR detector and inner decoder before they pass information to each other in order to avoid feedback of previously processed outputs; similar subtractions are performed in the SCCC decoder loop at the outputs of the inner and outer MAP decoders, but these are not shown in Fig. 2.

III. BCJR ALGORITHM FOR TDMR DETECTION

A. Trellis Construction

The grain state definition for the proposed BCJR detection algorithm is shown in Fig. 3. Each of the state subgrains can in theory take on one of the nine subgrain values A-I shown in Fig. 1; however, grain connectivity restrictions shown in Table I restrict the total number of current grain states (s'_0, s'_1) to 39. The bit “X” is feedback from the previously detected row; the probabilities associated with the X bit are used to modify the state transition probabilities in a soft-decision feedback scheme somewhat similar to the 2D intersymbol interference (ISI) equalization algorithm described in [6].

Fig. 4 shows the data states for the two-row BCJR trellis.

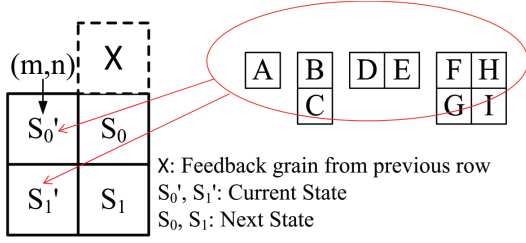


Fig. 3. The grain state definition for the two-row TDMR BCJR detector for the four-grain DGM of Fig. 1.

TABLE I. CONNECTIVITY RESTRICTIONS BETWEEN s'_0 AT LOCATION (M,N) AND s'_1 AT $(M+1,N)$, AND BETWEEN s'_0 AT (M,N) AND s_0 AT $(M,N+1)$.

$s'_0: (m,n)$	$s'_1: (m+1,n)$	$s_0: (m,n+1)$
A	A, B, D, E, F, H	A, B, C, D, F, G
B	C	A, B, C, D, F, G
C	A, B, D, E, F, H	A, B, C, D, F, G
D	A, B, D, E, F, H	E
E	A, B, D, E, F, H	A, B, C, D, F, G
F	G	H
G	A, B, D, E, F, H	I
H	I	A, B, C, D, F, G
I	A, B, D, E, F, H	A, B, C, D, F, G

This state-input block scans through three input rows of a given 2D data block row-by-row in raster order, corresponding to the scan order of typical shingled writing heads proposed for TDMR [7]. The trellis branch outputs y_{k0} and y_{k1} are the bits actually read from code bit locations (m, n) and $(m + 1, n)$, which are also the location of the current state subgrains (s'_0, s'_1) . The data states capture the bit over-write property of TDMR, i.e., the relation between the trellis branch outputs (y_{k0}, y_{k1}) and the corresponding input code bits that were originally written on the disk. For example, output y_{k0} may equal input $u_{m,n}$ or “future” input $u_{m,n+1}$ depending on whether grain states (s'_0, s_0) are occupied by single grains (such as AA, AB, etc.) or a connected grain (such as DE or FH).

Although trellis states can be constructed as the Cartesian product of the media and data states, in fact there is only one possible data state for each of the 39 media states shown in Table I, so that the overall trellis needs only 39 states. This is one of the advantages of the subgrain labeling scheme in Fig. 1: it reduces the number of states in the initial trellis construction compared to the scheme in [3], which constructs the trellis as the Cartesian product of media and data states. If we were to use the subgrain labeling scheme to define the current and next states (s'_0, s_0) employed in [3], we would require only 9 states labeled A-I for s'_0 , as opposed to the 16 states required in the initial trellis construction in [3]. However, as pointed out in [3], combination of equivalent states in their trellis reduces the number of states from 16 to 6. Hence, our subgrain labeling scheme does not give a minimum state trellis; however, it does provide a relatively straightforward method of constructing trellises for multi-row TDMR BCJR detectors that are reasonably efficient in terms of state complexity and that are free of geometrically invalid states.

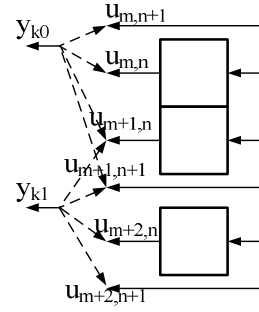


Fig. 4. Data states for the 2-row BCJR detector.

B. Computation of BCJR Probabilities

In the BCJR algorithm, the first and most important step is to compute the gamma state transition probability [4]:

$$\gamma_i(\mathbf{y}_k, s', s) = P(\mathbf{y}_k | \mathbf{U} = \mathbf{i}, S_k = s, S_{k-1} = s') \times P(\mathbf{U} | s, s') \times P(s | s'). \quad (1)$$

Note that the *a priori* probabilities from the inner MAP decoder have been left out of (1). We now describe the computation of each of the factors in the gamma probability. In (1), grain state transition probabilities $P(s | s')$ can be computed from Table I and the grain probabilities shown in Fig.1. The $P(s | s')$ probabilities can be stored in a 39×39 table. Since the $P(s | s')$ table is very sparse, we show only one typical row in Table II. In Table II, $P(\bar{B}, \bar{F})$, $P(\bar{B})$, $P(\bar{F})$ specify probabilities of the feedback pixel ‘X’ in Fig.3, where ‘ \bar{B} ’ means ‘not equal to B’. These feedback probabilities are computed from the LLRs from the detection of previous rows. Figure 5(a) shows an example of the grain states involved in the state transition probability $P(DF|AA)$, which is calculated as:

$$P(DF|AA) = P_4 \cdot P_3 \cdot P(\bar{B}, \bar{F}), \quad (2)$$

where the last factor is the probability that the feedback subgrain X is neither a B nor an F subgrain.

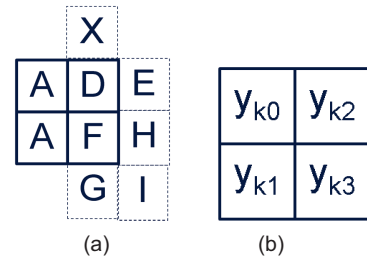


Fig. 5. (a) Grain states involved in the transition probability $P(DF|AA)$; note that the two A subgrains are located at positions (m, n) and $(m + 1, n)$, corresponding to the current state (s'_0, s'_1) in Fig. 3. (b) Outputs involved in the conditional channel probability $P(\mathbf{y}_k | \mathbf{U} = \mathbf{i}, S_k = s, S_{k-1} = s')$; note that y_{k0} and y_{k1} are located at positions (m, n) and $(m + 1, n)$, respectively.

The computation of the feedback subgrain probabilities $P(X = B)$ and $P(X = F)$ proceeds as follows. We define the joint probability λ in the usual way [4]:

$$\lambda_k^i(s) = P(\mathbf{U}_k = \mathbf{i}, S_k = s, \mathbf{y}_1^{N_r}) = \sum_{s'} \alpha_{k-1}(s') \cdot \gamma_i(\mathbf{y}_k, s', s) \cdot \beta_k(s), \quad (3)$$

TABLE II. CONDITIONAL PROBABILITIES OF NEXT STATES GIVEN THAT THE CURRENT STATE IS 'AA'.

s	$P(s s' = AA)$	s	$P(s s' = AA)$	s	$P(s s' = AA)$	s	$P(s s' = AA)$
AA	$P_1 \cdot P_1 \cdot P(\bar{B}, \bar{F})$	AB	$P_1 \cdot P_2 \cdot P(\bar{B}, \bar{F})$	AD	$P_1 \cdot P_3 \cdot P(\bar{B}, \bar{F})$	AE	0
AF	$P_1 \cdot P_4 \cdot P(\bar{B}, \bar{F})$	AH	0	BC	$P_2 \cdot P(\bar{B}, \bar{F})$	CA	$P_1 \cdot P(B)$
CB	$P_2 \cdot P(B)$	CD	$P_3 \cdot P(B)$	CE	0	CF	$P_4 \cdot P(B)$
CH	0	DA	$P_1 \cdot P_3 \cdot P(\bar{B}, \bar{F})$	DB	$P_2 \cdot P_3 \cdot P(\bar{B}, \bar{F})$	DD	$P_3^2 \cdot P(\bar{B}, \bar{F})$
DE	0	DF	$P_4 \cdot P_3 \cdot P(\bar{B}, \bar{F})$	DH	0	EA	0
EB	0	ED	0	EE	0	EF	0
EH	0	FG	$P_4 \cdot P(\bar{B}, \bar{F})$	GA	$P_1 \cdot P(F)$	GB	$P_2 \cdot P(F)$
GD	$P_3 \cdot P(F)$	GE	0	GF	$P_4 \cdot P(F)$	GH	0
HI	0	IA	0	IB	0	ID	0
IE	0	IF	0	IH	0		

where we estimate two input bits $\mathbf{U}_k = (u_{0k}, u_{1k})$ at each trellis stage, the α and β probabilities are defined as in [4], and the notation $\mathbf{y}_1^{N_r}$ refers to the entire sequence of received output vectors along one row of length N_r . The LLRs $L(B)$ and $L(F)$ are computed as:

$$L(B) = \log \left[\frac{\sum_i \lambda_k^i(s=BC)}{\sum_i \lambda_k^i(s \neq BC)} \right] \quad (4)$$

$$L(F) = \log \left[\frac{\sum_i \lambda_k^i(s=FG)}{\sum_i \lambda_k^i(s \neq FG)} \right],$$

where it is understood that the lambda probabilities are those for the feedback subgrain X. The probabilities $P(X = B)$ and $P(X = F)$ are then recovered from the LLRs in the usual manner as

$$P(X = S) = \frac{\exp(L(S))}{1 + \exp(L(S))}, \quad (5)$$

where S is either B or F .

The probability $P(\mathbf{U} | s, s')$ in (1) is equal to 1/4, since the two coded bits in the input vector \mathbf{U} are assumed to be independent of each other (due to the interleaver) and of the grain states.

The conditional probabilities $P(\mathbf{y}_k | \mathbf{U} = \mathbf{i}, S_k = s, S_{k-1} = s')$ of the k th output vector $\mathbf{y}_k = (y_{k0}, y_{k1}, y_{k2}, y_{k3})$ shown in Fig. 5(b) are stored in a three dimensional array of size $16 \times 4 \times 39 = 2496$, as the output vector \mathbf{y}_k depends only on the two element input vector and on the previous state $S_{k-1} = s'$. In these probabilities, the input bits u_{k0} and u_{k1} are assumed to be located at (m, n) and $(m + 1, n)$, i.e., input bit u_{ki} is co-located with output bit y_{ki} , for $i = 0, 1$. The conditional probabilities $P(\mathbf{y}_k | \mathbf{U} = \mathbf{i}, S_k = s, S_{k-1} = s')$ can take only the values of 0, 0.5, 0.25, or 0.125; in fact, most of the probabilities in the table are equal to 0. We now provide examples of each of these four cases.

First, $P(\mathbf{y}_k | \mathbf{U} = \mathbf{i}, S_{k-1} = FG)$ equals zero whenever the four output bits in \mathbf{y}_k are not all equal, because in this case a single FGHI grain occupies the entire state block (s', s) of Fig. 3, and hence all the output bits must be equal. This case can be detected easily because the algorithm examines two rows and two columns at a time. Second, for the same value of $S_{k-1} = FG$ as above, $P(\mathbf{y}_k | \mathbf{U} = \mathbf{i}, S_{k-1} = FG) = 0.5$ whenever the four output bits in \mathbf{y}_k are all equal, because in this case all four of these bits are determined by the single

input bit at $(m + 1, n + 1)$, which is independent of either of the two given input bits u_{k0} or u_{k1} at locations (m, n) and $(m + 1, n)$. This is the only case in which the conditional probability takes the value 0.5. Third, $P((u_{k0}, u_{k1}, y_{k2}, y_{k3}) | (u_{k0}, u_{k1}), S_{k-1} = AA) = 0.25$ for any pairs (u_{k0}, u_{k1}) and (y_{k2}, y_{k3}) , since in this case with $S_{k-1} = AA$ the input bits are written directly on the output bit locations, and the probability is equal to 0.25 as long as the inputs and outputs agree. (The presence of the two ‘‘don’t care’’ bits y_{k2} and y_{k3} , which can assume four arbitrary values, accounts for the value of 0.25.) Also, $P(\mathbf{y}_k | \mathbf{U} = \mathbf{i}, S_{k-1} = DD) = 0.25$ whenever $y_{k0} = y_{k2}$ and $y_{k1} = y_{k3}$, and 0 otherwise, since in this case the two state rows are both DE grains, so that outputs y_{k0} and y_{k1} are determined by the two inputs at $(m, n + 1)$ and $(m + 1, n + 1)$ respectively, which can assume a total of four different values. The only possible next state after DD is EE, so at the next shift of the state register we will have the case $P((u_{k0}, u_{k1}, y_{k2}, y_{k3}) | (u_{k0}, u_{k1}), S_{k-1} = EE) = 0.25$, similar to the case above where $S_{k-1} = AA$. Fourth, $P(\mathbf{y}_k | \mathbf{U} = \mathbf{i}, S_{k-1} = DB) = 0.125$ whenever $y_{k0} = y_{k2}$, and 0 otherwise, since in this case there is a DE grain occupying the first state row (s'_0, s_0) and a BC grain occupying positions $(m + 1, n)$ and $(m + 2, n)$. Thus, outputs y_{k0} and y_{k1} are determined by the inputs at $(m, n + 1)$ and $(m + 2, n)$, which take four different values; the ‘‘don’t care’’ bit y_{k3} can also assume two independent arbitrary values.

IV. SIMULATION EXPERIMENTS

In this section we describe the details and give the results of Monte-Carlo simulations of the system shown in Fig. 2. The goal of the simulation experiments is to find the highest SCCC code rate that allows decoding at a BER of 10^{-5} or lower, as higher code rates correspond to a higher density of user bits (measured in user bits per magnetic grain) on the magnetic disk.

A. TDMR/SCCC Interface and Iteration Schedule

With reference to the TDMR/SCCC detector/decoder shown in the bottom half of Fig. 2, the LLRs output from the TDMR detector have a bimodal conditional PDF with two peaks immediately to the right and left of zero, as shown in Fig. 6, which shows the experimental LLR PDF conditioned on correct bit values of +1. The LLRs around zero correspond to bits with low to medium reliability; there is also a delta function at +100 (not shown in Fig. 6) that corresponds to

high reliability bits estimated by the TDMR detector. We find experimentally that modeling the central bimodal PDF as a Gaussian as shown in Fig. 6, and using that Gaussian as the conditional channel PDF in the SCCC decoder’s BCJR algorithm, gives good results for the SCCC decoder. When no iterations are done between the TDMR detector and the SCCC decoder, we find that optimizing the mean and the variance of the Gaussian model depending on the value of probability P_2 (the probability of BC grains, and also of DE grains since we assume $P_2 = P_3$) gives improved BER performance of the combined detector/decoder. With iteration between the TDMR and SCCC, we find that we can fix the mean and variance of the Gaussian model to be 1.0 and 1.69 respectively, for all values of P_2 .

With no TDMR/SCCC iterations, the SCCC decoder loop is run 30 times. This can be reduced by using one of the several stopping criteria that have been developed for turbo codes (e.g., [8]). With iteration between the TDMR and SCCC, we find experimentally that performing eight inner iterations of the SCCC decoder loop for each outer iteration of the entire TDMR/SCCC loop gives the best overall BER performance. The number of outer iterations required for successful decoding at a BER of 10^{-5} varies depending on value of P_2 (which also determines the code rate) and on the individual block being decoded, but never exceeds thirty outer iterations; the average number of outer iterations is close to eight for all values of P_2 except $P_2 = 0$, where it is two. In place of an SCCC stopping criteria, we check each decoded block for errors against the known transmitted block, and stop decoding when zero errors are detected; although this is not possible in an actual system, we believe that using a stopping criteria would give similar results for the maximum and average numbers of iterations required.

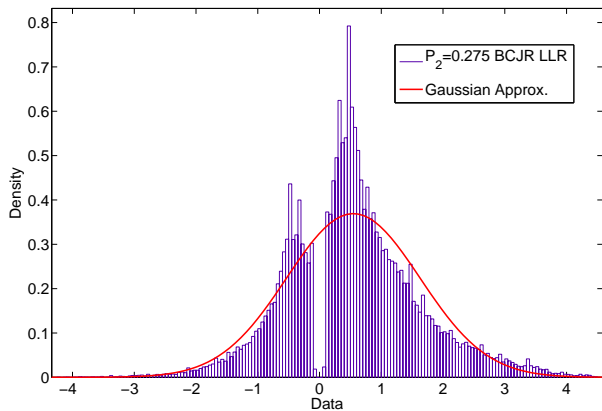


Fig. 6. Experimental PDF of TDMR output LLRs conditioned on +1 bits, and best fit Gaussian PDF.

B. Monte Carlo Simulations

Each block of 32768 data bits is encoded into a block of $32768/r$ coded bits, where r is the code rate. For each block of coded bits, a random grain image of size $256 \times 512 = 131072$ coded bits is generated, corresponding to a code rate of $r = 1/4$; higher or lower code rates are handled by deleting or adding rows of length 512 from the random grain image.

The random grain image is generated using the greedy tiling algorithm described in [2], which places the largest grains first and then fills the holes between with smaller grains. However, at values of P_2 greater than about 0.36, it becomes difficult to generate large random grain images because there are not enough 1×1 grains to fill the holes between larger grains. To overcome this, when P_2 is above 0.36 we generate a large set of 16×16 bit random sub-images, and then fill the large grain image with these 16×16 sub-images by randomly choosing sub-images from the generated set. Once the random grain image is generated, the coded bits are level shifted so that the values $(0, 1)$ map to the values $(-1, 1)$, and then the level shifted bits are written onto the grain image in row-by-row raster scan order, following the grain-overwrite rule that the last bit written onto a given grain determines that grain’s polarity. The written grain image then flows into the TDMR/SCCC detector/decoder. A sufficient number of data bit blocks are sent so that a BER of 10^{-5} or higher can be reliably measured. In order to facilitate trellis termination, we surround each written grain image by a boundary of 1×1 “A” grains that have all been written to -1 . To our knowledge, these simulation conditions are exactly the same as those in [3], except that we are unsure how that paper handled grain image generation at values of P_2 above 0.36.

The Monte-Carlo simulation results are shown in Fig. 7. The figure’s horizontal axis is the probability P_2 , and the vertical axis is the number of user bits per grain, which is equal to twice the code rate since we assume a density of two coded bits per grain. The blue line at 0.5 user bits/grain corresponds to the bit density that can be achieved by using a rate 1/4 repetition code [2]. The upper and lower bounds on the channel capacity of the four-rectangular-grain TDMR channel (from [2]) are also shown. The results achieved by the non-iterative TDMR/SCCC system of [3] are shown in blue dots; the corresponding results for the non-iterative system in the present paper are shown in red squares, with the percentage rate gain relative to [3] shown immediately adjacent to each red square. The largest rate gain of 6.67% occurs at $P_2 = 0$, and actually exceeds the lower capacity bound. The rate gains decrease to around 5% for P_2 between 0.2 and 0.3, and then decrease further until there is actually a rate loss of about 1.1% at $P_2 = 0.5$. We believe the rate gains are largely due to processing two rows (and four outputs) at a time in our BCJR algorithm; this allows, e.g., easy elimination of potential FGHI grain states by checking for agreement between all four bits in the grain. We are unsure about why the performance dips at $P_2 = 0.5$; possibly it is due to our using a somewhat different method of generating random grain images at high values of P_2 than that used in [3].

The performance of our TDMR/SCCC system with iterative processing is shown in black triangles in Fig. 7, with the rate gains relative to [3]. The rate gains due to iterative processing are substantial. Again the best result is at $P_2 = 0$, where there is a 13.4% rate gain; in fact, the point at $P_2 = 0$ attains 92.5% of the average of the channel capacity upper and lower bounds, which is a rough approximation of the true channel capacity. The rate gains in the most-difficult-to-handle middle range of P_2 between 0.2 and 0.3 are around 10%; significantly, the achieved rates with iterative processing are everywhere above the performance of the rate 1/4 repetition code. Also interesting is the performance at $P_2 = 0.5$, where

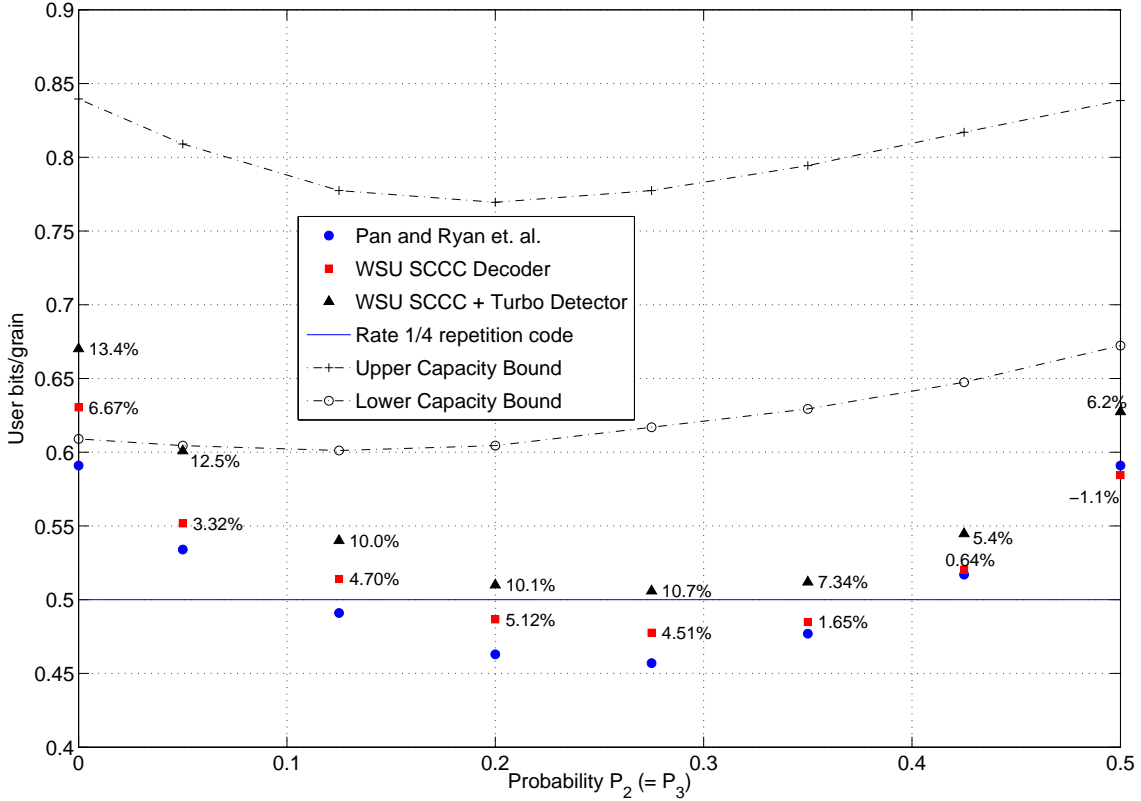


Fig. 7. TDMR detection and decoding simulation results.

a rate gain of 6.2% is achieved; iterative processing has raised the rate there by over 7.3% compared to non-iterative processing. The proposed iterative system achieves at least 72% of the average of the channel capacity upper and lower bounds at all values of P_2 ; the corresponding figure for [3] is 65%.

V. CONCLUSION

This paper has presented a system for detection and decoding of bits on the four-rectangular-grain TDMR channel, using a novel two-row BCJR-based TDMR detector, together with SCCC error correction coding. Non-trivial gains in user bit density, especially at low values of the two-grain probability P_2 , are enabled by processing two rows and four outputs at a time in the TDMR detector. When iteration is allowed between the TDMR and SCCC, additional substantial density gains are enabled at all values of P_2 , albeit at a complexity cost of roughly six or seven times that of the non-iterative system, when the total numbers of SCCC and TDMR iterations are taken into account.

An interesting extension that we are currently pursuing involves splitting the TDMR BCJR detector into two detectors, one that runs over rows as in this paper, and the other that runs over columns. The two detectors can exchange soft bit and grain state information with each other and thereby possibly converge at higher code rates than either could alone, as

they together can exploit the two different (and somewhat independent) views of the TDMR channel. Similar row-column iteration strategies have worked well in iterative equalizers for 2D intersymbol interference channels (e.g., [6], [9]–[12]). Results of the row-column TDMR detector work will be reported in future publications.

ACKNOWLEDGMENT

This work was supported by NSF grants CCF-1218885 and CCF-0635390. The authors also wish to acknowledge useful discussions with Dr. Roger Wood of Hitachi Global Storage Technologies, San Jose, CA.

REFERENCES

- [1] R. Wood, M. Williams, A. Kavcic, and J. Miles, "The feasibility of magnetic recording at 10 terabits per square inch on conventional media," *IEEE Trans. Magnetics*, vol. 45, no. 2, pp. 917–923, Feb. 2009.
- [2] A. Kavcic, X. Huang, B. Vasic, W. Ryan, and M. F. Erden, "Channel modeling and capacity bounds for two-dimensional magnetic recording," *IEEE Trans. Magnetics*, vol. 46, no. 3, pp. 812–818, Mar. 2010.
- [3] L. Pan, W. E. Ryan, R. Wood, and B. Vasic, "Coding and detection for rectangular-grain TDMR models," *IEEE Trans. Magnetics*, vol. 47, no. 6, pp. 1705–1711, June 2011.
- [4] L. R. Bahl, J. Cocke, F. Jelinek, and J. Raviv, "Optimal decoding of linear codes for minimizing symbol error rate," *IEEE Transactions on Information Theory*, vol. 20, pp. 284–287, March 1974.

- [5] S. Benedetto, D. Divsalar, G. Montorsi, and F. Pollara, "Serial concatenation of interleaved codes: performance analysis, design, and iterative decoding," *IEEE Trans. Inform. Theory*, vol. 44, pp. 909–926, May 1998.
- [6] T. Cheng, B. J. Belzer, and K. Sivakumar, "Row-column soft-decision feedback algorithm for two-dimensional intersymbol interference," *IEEE Signal Processing Letters*, vol. 14, pp. 433–436, July 2007.
- [7] S. Greaves, Y. Kanai, and H. Muraoka, "Shingled recording for 2-3 Tbits per square inch," *IEEE Trans. Magnetics*, vol. 45, no. 10, pp. 3823–3828, Oct. 2009.
- [8] R. Y. Shao, S. Lin, and M. P. Fossorier, "Two simple stopping criteria for turbo decoding," *IEEE Trans. Commun.*, vol. 47, pp. 1117–1120, Aug. 1999.
- [9] X. Chen and K. M. Chugg, "Near-optimal data detection for two-dimensional ISI/AWGN channels using concatenated modeling and iterative algorithms," in *Proc. IEEE International Conference on Communications, ICC'98*, 1998, pp. 952–956.
- [10] M. A. Neifeld, R. Xuan, and M. W. Marcellin, "Communication theoretic image restoration for binary-valued imagery," *Applied Optics*, vol. 39, no. 2, pp. 269–276, Jan. 2000.
- [11] Y. Wu, J. A. O'Sullivan, N. Singla, and R. S. Indeck, "Iterative detection and decoding for separable two-dimensional intersymbol interference," *IEEE Trans. Magnetics*, vol. 39, no. 4, pp. 2115–2120, July 2003.
- [12] M. Marrow and J. K. Wolf, "Iterative detection of 2-dimensional ISI channels," in *Proc. Info. Theory Workshop*, Paris, France, Mar./Apr. 2003, pp. 131–134.